Reactive & Functional Polymers 69 (2009) 498–506

Contents lists available at ScienceDirect

Reactive & Functional Polymers

journal homepage: www.elsevier.com/locate/react

# Supramolecular structures of an amphiphilic hairy-rod conjugated copolymer bearing poly(ethylene oxide) side chain

Shao-Ching Liao [a], Chia-Sheng Lai [a], Di-Di Yeh [b], M. Habibur Rahman [c], Chain-Shu Hsu [b], Hsin-Lung Chen [a,*], Show-An Chen [a]

[a] Department of Chemical Engineering, National Tsing Hua University, Hsin-Chu 30013, Taiwan
[b] Department of Applied Chemistry, National Chiao Tung University, Hsin-Chu 30050, Taiwan
[c] Department of Chemistry, University of Rajshahi, Rajshahi 6205, Bangladesh

ARTICLE INFO

*Article history:*
Available online 2 April 2009

*Keywords:*
Amphiphilic hairy-rod copolymer
Conjugated polymer
Supramolecular structure
SAXS
Micelle

ABSTRACT

The structures of an amphiphilic conjugated graft copolymer, poly(2,3-diphenyl-5-(trimethylene-heptadeca(oxyethylene)-methoxy-phenylene vinylene) (denoted as $PVEO_{17}$) composing of a conjugated DP-PPV backbone and PEO side chains, in bulk and solutions with tetrahydrofuran (THF) and water have been investigated by small-angle X-ray scattering (SAXS). In bulk state, the DP-PPV main chains in $PVEO_{17}$ stacked to form flat disk microdomains dispersed in the PEO side-chain matrix. The corresponding wide angle X-ray scattering pattern revealed the existence of crystallinity of the PEO side chains. The structure of the polymer in solution was affected by the solvent quality and the polymer concentration. $PVEO_{17}$ chains were relatively well dispersed in THF. In aqueous solutions, however, the amphiphilic $PVEO_{17}$ chains aggregated significantly over the concentration range of 1–8 wt%, where the polymer was found to self-organize to form cylindrical micelles with the aggregation number increasing with the increase of concentration. The photophysical properties characterized by UV–Vis and photoluminescence spectroscopy were strongly affected by the aggregation state of the polymer.



## 1. Introduction

Copolymers composing of rodlike conjugated segment have drawn much attention recently. In particular, a combination of the rod unit with the flexible coil unit in the copolymer can give rise to a rich variety of interesting self-assembled nanostructures and properties. There are two basic classes of this type of rod-coil copolymers: (1) rod-coil block copolymer [1–5] where the rod block is attached covalently to a coil block at the chain end, and (2) hairy-rod copolymer [6–11] where the flexible chains are grafted to the rigid rodlike backbone at high density**.** In both cases, the driving force of microphase separation associated with the strong repulsion between the rod and coil units and the tendency of the rodlike chains to form liquid crystalline phases due to their anisotropic interaction may lead to complex phase behavior in both the bulk and solution state [2,3,7,8].

The present study reports the self-assembly behavior of an amphiphilic hairy-rod copolymer composing of a hydrophobic poly(phenylene vinylene) backbone and the hydrophilic poly(ethylene oxide) (PEO) side chains. Amphiphilic hairy-rod copolymers have been developed for realizing the aqueous processability of conjugated polymers for opto-electronic applications. Introducing ionic moiety onto the conjugated backbone is an effective approach for accomplishing the water solubility. Sulfonated poly(p-phenylene) derivatives (PPPs) are one of such a polyelectrolyte that has been investigated in detail for their self-assemblies in cast films and aqueous solution [12–14]. Sulfonted PPPs grafted with hydrophobic alkyl chains were found to aggregate into strands due to the balance between hydrophilic and hydrophobic interactions [8]. The size of the strands was controlled by the hydrophobic interactions between the alkyl chain and water. Films cast from aqueous solutions showed ordered packing of cylindrical micelles, where the micelles self-organized into hexagonal arrays. Gitsas et al. [15] have also investigated the melt structure of PPPs containing dodecyl side chain and sulfonate ester groups in the backbone as a function of temperature and pressure. These PPPs showed isotropic, liquid crystalline and glassy phases under certain conditions. Under the atmospheric pressure, a transformation from the liquid crystalline phase to the isotropic phase was accessible by heating. Increasing pressure was found to enhance the stability of the liquid crystalline phase.

Several hairy-rod polyelectrolytes tended to form clusters in aqueous solutions. Addition of surfactant could destabilize the clusters and leads to stable solutions [16]. Mixing surfactant with hairy-rod conjugated polyelectrolyte in the aqueous solution also

* Corresponding author. Tel.: +886 3 5721714; fax: +886 3 5738415.
*E-mail address:* hlchen@che.nthu.edu.tw (H.-L. Chen).

1381-5148/$ - see front matter © 2009 Elsevier Ltd. All rights reserved.
doi:10.1016/j.reactfunctpolym.2009.03.007

raised the cloud point and facilitated the formation of homogeneous films for optical application in wider temperature ranges [17].

A series of poly(2,3-diphenyl-1,4-phenylene vinylene) (DP-PPVs) with different side-chain derivatives have been synthesized successfully for organic light emitting diodes with high brightness and high efficiency [18]. The most intense emission usually locates at 551 nm along with two shoulders at 515 and 596 nm. These emissions belong to the yellow–green luminescence in the visible zone. With the interest in developing the DP-PPV with water solubility, we have successfully attached PEO to the DP-PPV backbone, generating a poly(2,3-diphenyl-5-(trimethylene-heptadeca(oxyethylene)-methoxy-phenylene vinylene) (denoted as $PVEO_{17}$) [18]. The chemical structure of $PVEO_{17}$ is shown below.

PEO is a well-known water-soluble polymer, which has been combined with other polymer structures to produce amphiphilic copolymers. Because of its amphiphilic property, $PVEO_{17}$ can be dissolved in both polar and non-polar solvents. In this work, we systematically study the self-assembly behavior of $PVEO_{17}$ in the bulk and solution state mainly by means of small angle X-ray scattering (SAXS). We will particularly focus on the aggregate structures of the copolymers in tetrahydrofuran (THF) and water and examine the effect of aggregation on the photophysical properties characterized by UV–Vis and photoluminescence (PL) spectroscopy.

## 2. Experimentals

### 2.1. Synthesis of monomer and polymer (Scheme 1[18])

#### 2.1.1. 2,5-Dicarbethoxy-3,4-diphenylcyclopentadienone (*1*)

Benzil (15 g, 71 mmol) and diethyl 1,3-acetonedicarboxylate (17.3 g, 86 mmol) were introduced into a flask followed by the addition of methanol (300 mL). Potassium hydroxide (4 g, 71 mmol) dissolving in ethanol (20 mL) was then dropped into the flask and stirred for 24 h. The precipitate was filtered and dried. The product was added into 80 mL acetic anhydride and concentrated sulfuric acid was added dropwise till the color of the mixture became orange. After 30 min of continuous stirring, distilled water was added and the product was filtered followed by recrystallization from methanol to give orange product of Compound **(1)**. Yield 85%, Mp: 106 °C and $^1$H NMR (500 MHz, $CDCl_3$): $\delta$ 1.146 (t, 6H, $-CO_2-CH_2CH_3$), 4.185 (q, 4H, $-CO_2-CH_2CH_3$), 6.990–7.336 (m, 10H, $-C_6H_5$). $^{13}$C NMR (75 MHz, $CDCl_3$): $\delta$ 14, 61.4, 119.9, 127.8, 129.0, 130.3, 131.0, 131.1, 162.2, 191.1. MS (EI-MS) m/z: 376 ($M^+$).

#### 2.1.2. Diethyl 2,3-diphenyl-5-propyl-chloride terephthalate (*2*)

Compound **(1)** (16.03 g, 40 mmol) and 5-chloro-1-pentyne (4 g, 40 mmol) were introduced into a flask and refluxed at 120 °C for 24 h. A yellow product of Compound **(2)** was obtained after cooling the crude product followed by purification by TLC method (*n*-hexane/ethyl acetate = 4/1). Yield 92%, Mp: 143–145 °C, $^1$H NMR (500 MHz, $CDCl_3$): $\delta$ 0.879 (t, 3H, $-CH_2CH_3$), 1.335–1.229 (m, 8H, $-OCH_2CH_2(CH_2)_4$), 1.782 (m, 2H, $-OCH_2CH_2$), 3.968 (t, 2H, $-OCH_2$), 4.861 (s, 1H, $-OH$), 6.844–7.443 (m, 8H, $-C_6H_4$). 1.3 (t, 6H, $COOCH_2CH_3$), 1.9 (m, 2H, Cl $CH_2CH_2CH_2$), 2.55 (t, 2H, Cl $CH_2CH_2CH_2$), 3.38 (t, 2H, Cl $CH_2CH_2CH_2$), 4.29 (m, 2H, $COOCH_2CH_3$), 7.22 (m, 2H, aromatic-*H*), 7.32 (m, 4H, aromatic-*H*), 7.48 (m, 4H, aromatic-*H*), 7.96 (m, 1H, aromatic-*H*). $^{13}$C NMR (75 MHz, $CDCl_3$): $\delta$ 44.4, 60.9, 127.7, 127.9, 129.3, 130, 133.8, 133.9, 136.5, 136.7, 139.7, 166. MS (EI-MS) m/z: 450 ($M^+$).

#### 2.1.3. Diethyl 2,3-diphenyl-5-(trimethylene-heptadeca (oxyethylene)-methoxy) terephthalate (*3*)

Poly(ethylene oxide) methyl ether (14.25 g, 20 mmol), sodium hydride (0,86 g), a small amount of potassium iodide and THF (150 mL) were placed in a flask. After 1 h of reflux, Compound **(2)** (8.86 g, 20 mmol) was added and refluxed for 72 h. The solution was concentrated to yield the solid product which was then dissolved in ethyl acetate followed by washing with 5% hydrochloric

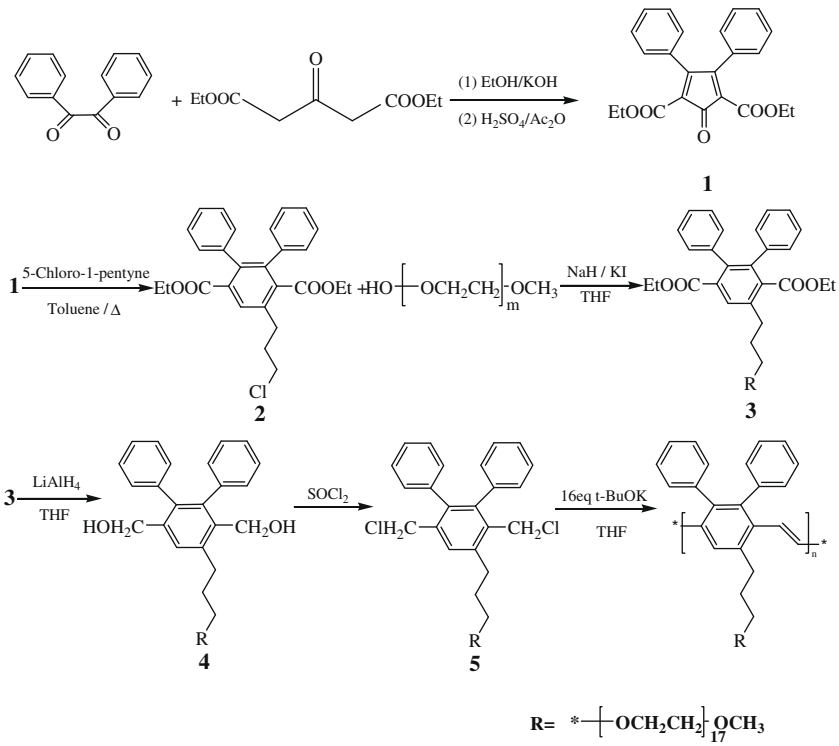


**Scheme 1.** Synthesis of $PVEO_{17}$.

acid and saturated sodium chloride aqueous solution. The organic layer was purified by TLC method (*n*-hexane/ethyl acetate = 2/1) to obtain Compound **(3).** Yield 64%, $^1$H NMR (500 MHz, $CDCl_3$): $\delta$ 1.3 (t, 6H, –$COOCH_2CH_3$), 1.79 (m, 2H, –$OCH_2CH_2CH_2$), 2.55 (t, 2H, –$OCH_2CH_2CH_2$), 3.24 (s, 3H, –$OCH_3$), 3.37 (t, 2H, –$OCH_2CH_2CH_2$), 3.54 (t, 72H, –$OCH_2CH_2OCH_2CH_2$ $OCH_2CH_2O$–), 4.29 (m, 4H, $COOCH_2CH_3$), 7.22 (m, 2H, aromatic-*H*), 7.32 (m, 4H, aromatic-H), 7.48 (m, 4H, aromatic-H), 7.96 (m, 1H, aromatic-H). $^{13}$C NMR (75 MHz, $CDCl_3$): $\delta$ 14.1, 25.8, 31.4, 59.3, 60.9, 70.2, 70.5, 72.0, 72.5, 72.7, 127.7, 127.9, 129.3, 130, 133.8, 133.9, 136.5, 136.7, 139.7, 166.

#### 2.1.4. 2,3-Diphenyl-5-(trimethylene-heptadeca (oxyethylene)-methoxy)-1,4-bis (hydroxymethyl) benznen (*4*)

Compound **(3)** (14.72 g, 10 mmol) was dissolved in THF (120 mL) followed by adding lithium aluminum hydrid (4.8 g, 120 mmol) in THF (120 mL) through syringe and the solution was refluxed for 72 h. The solution was then introduced dropwise into a saturated sodium hydroxide aqueous solution under low temperature till the color of the mixture became white. After a filtration, the organic layer was extracted from dichloromethane/saturated sodium chloride solution. The organic layer was concentrated to obtain the crude product which was subsequently purified by TLC method (*n*-hexane/ethyl acetate = 3/2) to produce a white solid of Compound **(4)**. Yield 36%, $^1$H NMR (500 MHz, $CDCl_3$): $\delta$ 1.79 (m, 2H, –$OCH_2CH_2CH_2$), 2.0 (s, 2H, –*OH*), 2.55 (t, 2H, –$OCH_2CH_2CH_2$), 3.24 (s, 3H, –$OCH_3$), 3.37 (t, 2H, –$OCH_2CH_2CH_2$), 3.54 (t, 72H, –$OCH_2CH_2OCH_2CH_2$ $OCH_2CH_2O$–), 4.1–4.2 (d, 4H, –$CH_2OH$), 7.0 (s, 1H, aromatic-*H*)), 7.22 (m, 2H, aromatic-*H*), 7.32 (m, 4H, aromatic-*H*), 7.48 (m, 4H, aromatic-*H*). $^{13}$C NMR (75 MHz, $CDCl_3$): $\delta$ 26.7, 31.7, 55.6, 59.3, 62.1, 70.2, 70.5, 72.0, 72.5, 72.7, 123.9, 127.7, 127.9, 129.3, 130, 133.6, 136.5, 137.4, 139.0.

#### 2.1.5. 2,3-Diphenyl-5-(trimethylene-heptadeca (oxyethylene)-methoxy)-1,4-bis(chloromethyl) benznen (*5*)

Compound **(4)** (1.7 g, 1 mmol) and thionyl chloride (3 mL) were introduced into a flask and reacted for 1 h. After removing the excess thionyl chloride, Compound **(5)** was purified form the crude product by TLC method (*n*-hexane/ethyl acetate = 5/3), Yield 73%. $^1$H NMR (500 MHz, $CDCl_3$): $\delta$ 1.79 (m, 2H, –$OCH_2CH_2CH_2$), 2.55 (t, 2H, –$OCH_2CH_2CH_2$), 3.24 (s, 3H, –$OCH_3$), 3.37 (t, 2H, –$OCH_2CH_2CH_2$), 3.54 (t, 72H, –$OCH_2CH_2OCH_2CH_2$ $OCH_2CH_2O$–), 4.2–4.3 (d, 4H, –$CH_2Cl$), 7.14 (s, 1H, aromatic-*H*)), 7.22 (m, 2H, aromatic-*H*), 7.32 (m, 4H, aromatic-*H*), 7.48 (m, 4H, aromatic-*H*). $^{13}$C NMR (75 MHz, $CDCl_3$): $\delta$ 25.9, 31.7, 33.9, 40.4, 59.3, 70.2, 70.5, 72, 72.7, 122.6, 125.4, 127.7, 127.9, 129.3, 129.2, 135.1, 136.5, 137.0, 137.3.

#### 2.1.6. Polymerization of poly(2,3-Diphenyl-5-(trimethylene-heptadeca(oxyethylene)-methoxy)-phenylene vinylene) ($PVEO_{17}$)

Monomer **(5)** (1.65 g, 1.48 mmol) was introduced into a flask and dissolved in THF. Then potassium t-butoxide (2.66 g, 0.02mole) in 15 mL THF was administered into the flask with the rate of 1.5 mL/min by a syringe. The solution was stirred at room temperature for 72 h. The resulting product was dropped into *n*-hexane twice and dialyzed 24 h by using THF as solvent. The purified polymer was dried in vacuo. The synthesized $PVEO_{17}$ had the weight average molecular weight ($M_w$) of ca. 14,600 with a polydispersity index of 2.1, as measured by a Viscotek VE2001 GPC using THF as the eluent and polystyrene as the standard. The lower $M_w$ compared to that of the general PPVs synthesized by the Gilch-route may result from the rather long PEO substituent that imposed a higher steric hindrance. From the value of $M_w$, we estimated that every $PVEO_{17}$ chain consisted of 12–13 PPV units.

### 2.2. Sample preparation.

The bulk sample of $PVEO_{17}$ was prepared by first dissolving the polymer in chloroform to the concentration of 1 wt% under stirring. The solution was then poured into a Petri dish and the solvent was allowed to evaporate at room temperature in a fume hood for 24 h to obtain the polymer film. For the preparation of the aqueous solution sample, $PVEO_{17}$ was first dissolved in THF at 40 °C for 30 min followed by agitating in an ultrasonic bath for 30 min and then stirring at room temperature for 24 h. The THF solution was added with a prescribed amount of deionized water. The resultant solution containing the cosolvent of THF and water was continuously stirred for overnight. The THF solvent was subsequently removed by natural evaporation at room temperature for 6 h. Three aqueous solutions with the polymer concentrations of 1, 5 and 8 wt% were prepared here.

### 2.3. Small-angle X-ray scattering (SAXS) measurements

SAXS experiments were conducted at beamline BL17B3 of the National Synchrotron Radiation Research Center (NSRRC), Taiwan. The beamline was configured for SAXS experiments using monochromatic radiation of wavelength $\lambda = 1.54$ Å and 8 KeV energy. The energy of the radiation was 8 keV and its corresponding wavelength was 1.55 Å. A two-dimensional Mar charge-coupled device (CCD) detector with 512 × 512 pixel resolution was used to collect scattering data. The sample-to-detector distance was ca. 2761.1 mm calibrated by PE standard and silver behenate. The $q$ range available for these measurements was 0.005–0.15 Å$^{-1}$. All scattering profiles had been corrected for background scattering and the scattering form solvent according to the polymer concentration.

### 2.4. UV–Visible and photoluminescence (PL) spectroscopy measurements

The photophysical properties of $PVEO_{17}$ in the solution state were investigated by UV–Vis and PL spectroscopy. Absorption spectra were recorded by a Perkin–Elmer model lambda 17 UV–VIS spectrometer. PL spectra were recorded using a Jobin Yvonb model FluoroMax-3 fluorescence spectrometer.

## 3. Results and discussion

### 3.1. Structure of $PVEO_{17}$ in the bulk state

The SAXS intensity profiles of block or graft copolymers in the bulk normally show a series of diffraction peaks associated with the long-range ordered nanostructures formed in the system. Fig. 1 displays the room-temperature SAXS profile of $PVEO_{17}$ in the bulk state. The scattering intensity decays monotonically without showing discernible peak, showing that the polymer does not form long-range ordered structures. A detailed examination of the SAXS profile in log–log plot reveals that the intensity shows a power-law dependence of $I(q) \sim q^{-3.7}$ in the low-$q$ region ($q < 0.04$ Å$^{-1}$) followed by the power law of $I(q) \sim q^{-2}$ between 0.04 and 0.095 Å$^{-1}$. The intensity shows a steeper decay after 0.1 Å$^{-1}$.

The $q^{-2}$ power-law dependence in the high-$q$ region indicates that $PVEO_{17}$ in the bulk self-organizes to form disklike domains [19] and the arrangement of these domains does not have apparent long-range order presumably because of the relatively high polydispersity of the polymer. However, the strong intensity upturn in the low-$q$ region implies that the disk domains aggregate to some extent, yielding a larger-scale heterogeneity. We propose

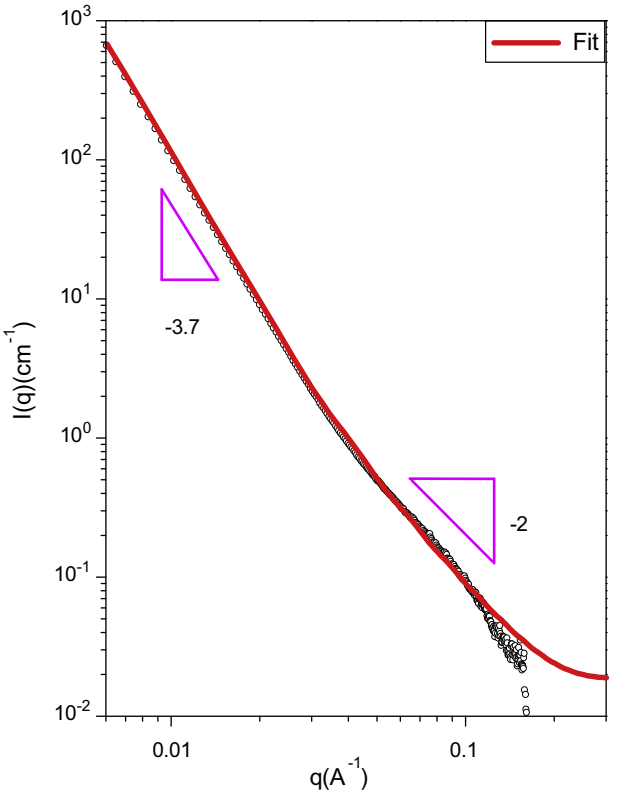


**Fig. 1.** The room-temperature SAXS profile in log–log plot of $PVEO_{17}$ in the bulk state. The solid curve represents the fit by Eq. (2).

that the repulsion between the rodlike DP-PPV backbone and the flexible PEO side chains induces a microphase separation, leading to disklike microdomains composing of DP-PPV unit dispersed in the PEO matrix (since the volume fraction of DP-PPV is only 0.25), as schematically illustrated in Fig. 2. The thickness of the disk domain, $L$, can be estimated using the Kratky–Porod equation for the effective $q$ range [20]:

$$I(q) = A\frac{2\pi}{q^2}(\Delta\rho^2)\mathrm{L}^2 e^{-\frac{\mathrm{L}^2}{12}q^2} \quad (1)$$

where $A$ is a constant. The thickness obtained from the slope of the $\ln(Iq^2)$ vs. $q^2$ plot is 22.4 Å.

To model the entire scattering profile, we used a combination of the Debye–Bueche equation [21,22] and cylinder form factor to fit the SAXS profile. The Debye–Bueche component is to account for the larger-scale heterogeneity associated with the disk aggregation. The model adopted here is hence expressed by:

$$I(q) = I_{cylinder}(q,R,L) + \frac{I_d(0)}{(1+\xi_d^2 q^2)^2} \quad (2)$$

where $\xi_d$ is the correlation length associated with larger-scale heterogeneity and $I_d(0)$ is the zero-angle scattering intensity prescribed by the D–B model. The cylindrical form factor is given by:

$$I_{cylinder}(q,R,\mathrm{L}) = (\Delta\rho)^2 NV^2 \times \int_0^{\frac{\pi}{2}} \left(\frac{\sin(qH\cos\varphi)}{qH\cos\varphi}\right)^2 \left(\frac{2J_1(qH\sin\varphi)}{qR\sin\varphi}\right)^2 \sin\varphi d\varphi \quad (3)$$

where $J_1$ is the first-order Bessel function, $\varphi$ is the angle between the cylinder axis and the scattering vector, and $H$ is the half of the disk thickness.

It can be seen from Fig. 1 that Eq. (2) yields a satisfactory fit to the experimental data. The radius and thickness of the disk domains obtained from the fit are 13.8 and 2.0 nm, respectively, and the correlation length is approximately 40.6 nm. The thickness of 2 nm implies that the disk is composed of two layers of DP-PPV main chains stacking normal to the disk surface. We propose that each layer includes a DP-PPV backbone (which contributes ca. 6 Å to the thickness) plus the three methylene units in the alkyl group of the side chain (which contribute ca. 3 Å to the thickness).

Since PEO is a crystalline polymer, it would be of interest to examine if the EO side chains attached to the rodlike DP-PPV backbone are crystallzible in the bulk state. Fig. 3 shows the wide-angle X-ray scattering (WAXS) pattern of $PVEO_{17}$ in the bulk. The WAXS pattern displays several diffraction peaks and a halo at around 1.54 Å$^{-1}$. The diffraction peaks are consistent with the characteristic reflections of PEO crystal [23]; therefore, crystallization of a fraction of the PEO side chains in $PVEO_{17}$ did take place in the bulk state. The strong scattering peak situating at 2.05 Å$^{-1}$ (corresponding to a Bragg spacing of 3.06 Å) which cannot be assigned to PEO crystal diffraction, is considered to stem from the highly stable π–π complex formed by the DP-PPV main chains in the dislike microdomains [24].

### 3.2. Structure of $PVEO_{17}$ in the solution state

We have investigated the structures of $PVEO_{17}$ in two solvents, namely, THF and water. THF is a moderately good solvent for PEO and a relatively good solvent for DP-PPV, while water is a good solvent for PEO but non-solvent for DP-PPV. The X-ray scattering length densities (SLD) of the DP-PPV backbone, PEO side chain, THF and water are $8.91\times10^{-6}$, $1.01\times10^{-5}$, $9.41\times10^{-6}$ and $8.38\times10^{-6}$ Å$^{-2}$, respectively. In THF where $PVEO_{17}$ is expected to be dissolved well, THF molecules may swell the PEO side chains, thereby reducing the SLD of the side chain region. In this case, the THF-swollen PEO side chains may display similar SLD to that of the backbone, such that the $PVEO_{17}$ chains may be considered to possess a uniform SLD and the contrast between the polymer chain and THF gives rise to the X-ray scattering. In the aqueous solution, the SLD of the side chain region may also be reduced due to the penetration of water; however, the resultant SLD is still expected to be obviously larger than that of the backbone. Consequently, the polymer chains or their micellar aggregates are considered to possess the core-shell structure for the modeling of the corresponding SAXS profiles.

Fig. 4 displays the SAXS profile of 1 wt% $PVEO_{17}$/THF solution. The SAXS profile of the aqueous solution is also shown for comparison. Both scattering profiles show upturns in the low-$q$ region, which correspond to the asymptotic power law of $I(q)\sim q^{-\alpha}$ with $\alpha = 2.3$ and 3 for water and THF solutions, respectively. The intensity upturn indicates the presence of inter-chain aggregation in

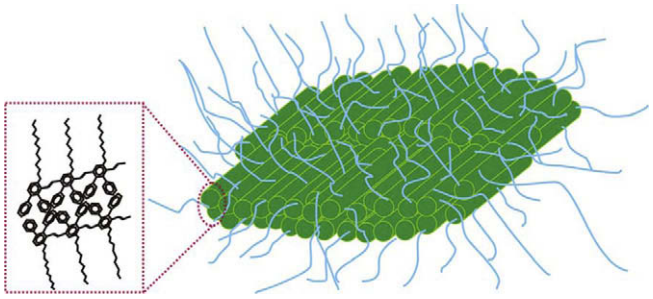

**Fig. 2.** Schematic illustration of the disk microdomains formed by $PVEO_{17}$. We propose that the repulsion between the rodlike DP-PPV backbone and the flexible PEO side chains induces a microphase separation, leading to disklike microdomains composing of DP-PPV unit dispersed in the PEO matrix.

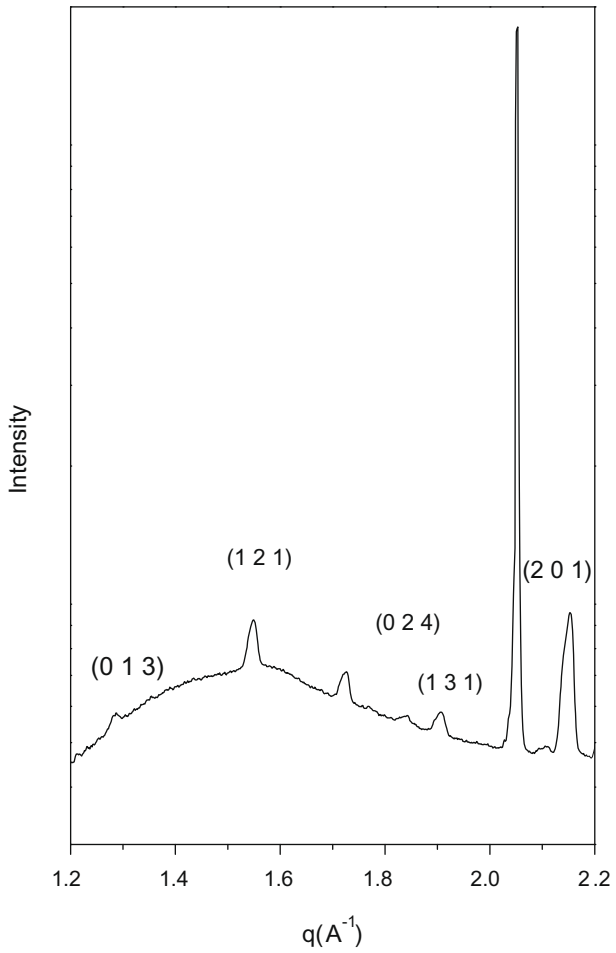


**Fig. 3.** WAXS profile of $PVEO_{17}$ in the bulk, showing the occurrence of crystallization of a fraction of the PEO side chains in $PVEO_{17}$. The strong scattering peak situating at 2.05 $Å^{-1}$ (corresponding to a Bragg spacing of 3.06 Å) is attributed to the highly stable π–π complex formed by the DP-PPV main chains.

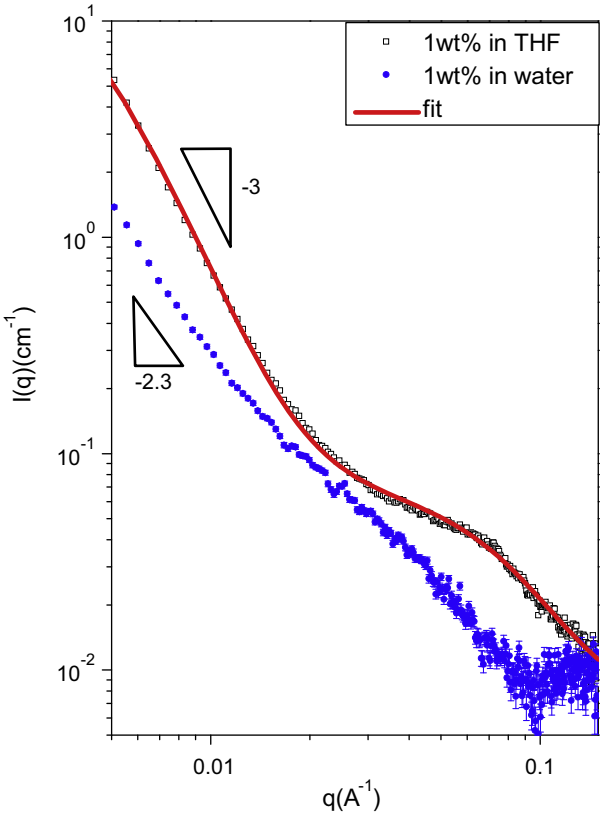


**Fig. 4.** The room-temperature SAXS profiles in log–log plots of 1.0 wt% solutions of $PVEO_{17}$ in THF and water. The solid curve superposing on the profile of THF solution represents the fit by Eq. (2).

both solutions. The scattering intensity of THF solution starts to level off at $q \sim 0.03$ $Å^{-1}$, but it experiences a steeper drop beyond 0.07 $Å^{-1}$. The scattering profile of THF solution can also be modeled satisfactorily by Eq. (2) (*cf.* the solid curve superposing on the scattering profile); however, here the cylinder form factor is associated with the individual rodlike chains of $PVEO_{17}$ considering the small values of the radius (1.75 nm) and the length (6.65 nm) of the cylinder obtained from the model fitting. The length of the rod is close to that (6.5 nm) determined from the molecular weight of $PVEO_{17}$ assuming fully extended conformation. Considering that the fully extended length of the PEO side chains with 17 monomer units is ca. 6.0 nm, the small radius of 1.75 nm of the rodlike chain implies that the side chains in $PVEO_{17}$ dispersed in THF are hence quite coiled.

The intensity upturn at low-$q$ signals that the rodlike $PVEO_{17}$ chains may still aggregate in the solution and the characteristic correlation length of the aggregates obtained from the model fitting is ca. 25 nm.

The structure of $PVEO_{17}$ in the aqueous solutions with three concentrations, i.e., 1, 5 and 8 wt%, at room temperature are studied by SAXS. Fig. 5 displays the SAXS profiles of the three solutions. All scattering profiles show upturns in the low-$q$ region, which again reveals the existence of a larger-scale inhomogeneity. The exponent of the corresponding power law is slightly smaller for the 8 wt% solution (close to $q^{-2}$) compared with that of the 1 and 5 wt% solutions.

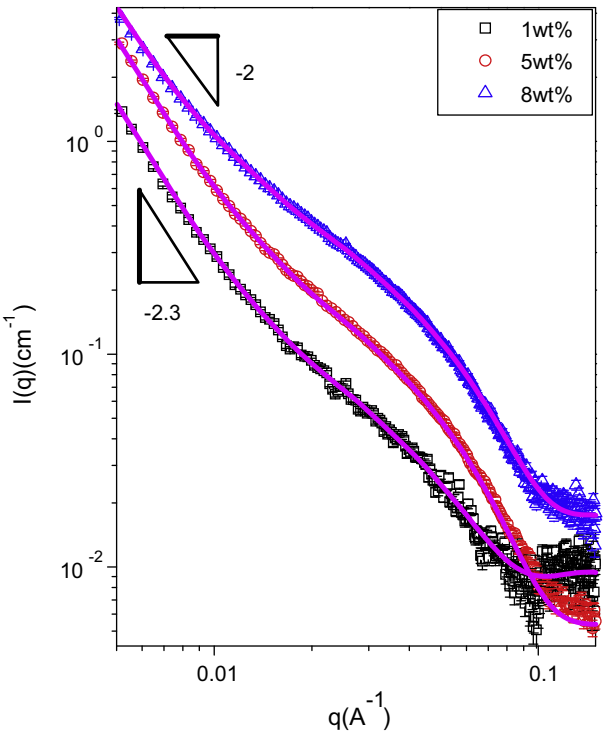


**Fig. 5.** Room-temperature SAXS profiles of $PVEO_{17}$ aqueous solutions with different concentrations. The solid curves superposing on the profiles are the fits by Eq. (4).

Since the PEO side chain is hydrophilic and the DP-PPV backbone is hydrophobic, we expect $PVEO_{17}$ chains to aggregate to form micelles in water. Cylinder is the most plausible micelle geometry considering the rodlike nature of the polymer chain. In this case, the DP-PPV backbone forms the core of the micelle, while the PEO side chains constitute the shell or corona that shield the core from being contact with water, as schematically illustrated in Fig. 6a.

According to the foregoing discussion, the SLDs of the water-swollen PEO shell and the DP-PPV core should be quite different; therefore, the form factor of the micelle should be described by the core-shell cylinder form factor. We attempt to verify the core-shell cylindrical micelle structure by fitting the experimental SAXS curves by the combination of the core-shell cylinder form factor and Debye–Bueche equation which accounts for the larger-scale heterogeneity arising from the clustering of the micelles (that gives raise to the intensity upturn at low-$q$). The equation used for the model fitting is hence expressed as

$$I(q) = I_{cs}(q, R_c, t_s, L) + \frac{I_d(0)}{(1 + \xi_d^2 q^2)^2} \quad (4)$$

where $I_{cs}(q, R_c, t_s, L)$ is the core-shell cylinder form factor [25] with $R_c$, $t_s$ and $L$ being the radius of the core, thickness of the shell and length of the cylinder, respectively. It can be seen from Fig. 5 that Eq. (4) does yield satisfactory fits to the experimental data. The structure parameters obtained from the model fittings for the three concentrations are listed in Table 1.

It is seen from Table 1 that the core radius of the micelle increases with the increase of concentration. The length of the micelle also appears to increase with concentration; however, considering that the corresponding error bars are relatively large and the difference in length between two concentrations is less than the length of a $PVEO_{17}$ rod, the increase of the micelle length is not considered to be physically meaningful. Considering that the width of the DP-PPV backbone is ca. 6 Å, we may estimate the number of DP-PPV chains contributing to the cross section of the micelle core, $N_r$, by $N_r = \frac{\pi \times R_c^2}{\pi (3)^2}$. The values of $N_r$ are also shown in Table 1. Moreover, we have obtained the chain length of $PVEO_{17}$ of ca. 65 Å from analysis of the SAXS data of the THF solution; the number of the chains packing along the long axis of the cylinder micelle, $N_L$, may hence be estimated via $N_L = \frac{L}{65}$, which is about five. Our analysis shows that the number of PPV chains occupying the micelle cross section ($N_r$) increases with increasing concentration. Fig. 6b schematically illustrates the cross-section packing of the polymer chains forming the micelle.

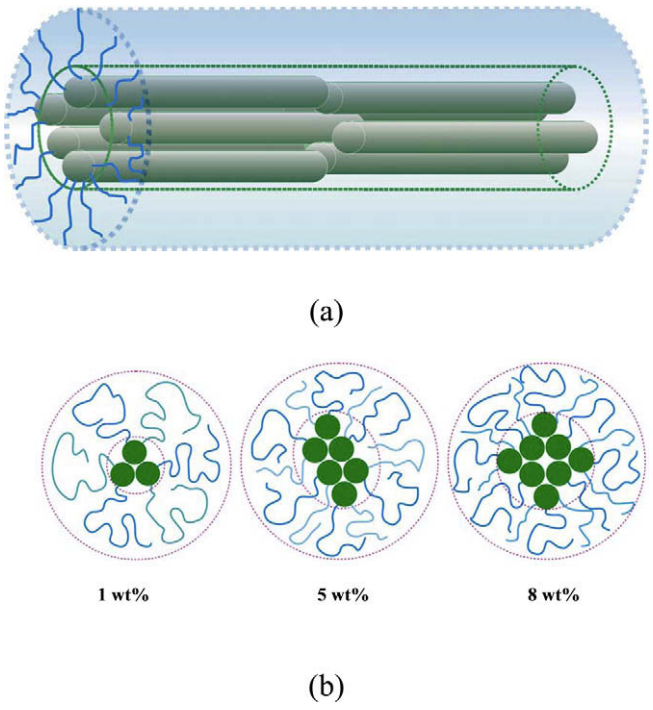


**Fig. 6.** (a) Schematic illustration of the core-shell cylinder micelles formed by $PVEO_{17}$ in aqueous solution. (b) schematic illustration of the cross section of the micelle formed at different concentrations.

Consequently, we conclude that $PVEO_{17}$ chains self-assemble to form cylindrical micelles due to the balance between hydrophobic and hydrophilic interactions. It is noted that the thickness of the shell composing of the water-swollen PEO side chains decreases with increasing polymer concentration. We speculate that at the higher concentration, the larger number of the PEO chains per micelle leads to prevalent inter-chain interaction between PEO side chains attached to the micelles. It is known that PEO undergoes aggregation in water at higher concentration [26,27]. Therefore, the stronger aggregation of the PEO chains in the shell region at higher concentration expels a larger amount of water out of this region, and hence reduces the shell thickness. Over the concentration range studied, the PEO side chains in the shells of different micelles also undergo aggregation (i.e., intermicellar aggregation), leading to clusters of the micelles that give rise to the upturns of SAXS intensities in the low-$q$ region. It is known that PEO may undergo aggregation in aqueous solution and several hypotheses have been proposed for the origin of PEO aggregation in water, including the presence of impurities [28], the formation of hydrogen bond [29] and the formation of complex entities associated with the presence of residual water molecules [30] and hydrophobic interactions [31].

### 3.3. Photophysical properties

Fig. 7 shows the UV–Vis spectra of $PVEO_{17}$ in the dilute solutions with THF and water (concentration = 0.05 wt%). The absorption peak is red shifted for the water solvent ($\tau$ = 1.85) relative to that for the THF solvent ($\tau$ = 1.63). Peaks associated with $\pi$–$\pi^*$ transition are generally shifted to longer wavelengths with increasing polarity of the solvent. Usually the bathochromic shift originates from the attractive polarization forces between the solvent and the absorber that tends to lower the energy levels of both the unexcited and the excited states [32]. However, this is not the plausible explanation for the bathochromic shift of the aqueous solution, because the absorber DP-PPV is hydrophobic such that the interaction between PPV and water is repulsive. A plausible interpretation for UV bathochromic shift is that the effective conjugate length of $PVEO_{17}$ is increased due to the formation of micellar aggregates in water solution [33] compared to that of the better dispersed molecules in THF solution.

Fig. 8 displays the PL spectra of $PVEO_{17}$ in THF solutions with various concentrations. The spectrum is virtually independent of concentration over the concentration range studied (0.001–1 wt%); therefore, the PL emission is considered to be dominated by the single chromophores. It should be noted that tetrahedral defects usually exist in the conjugated polymers such as PPVs synthesized by the Gilch-type polymerization [34] and these defects act as conjugation interrupters. Considering that the polydispersity (2.1) of $PVEO_{17}$ used in this study is relatively large, oligomeric chains should exist. However, the photoluminescence from these short chains may not be observed because of the energy transfer from the shorter conjugating segments to the longer ones [35–37] and further to the aggregates [38].

The PL spectrum of $PVEO_{17}$/water solution changes obviously relative to that of the THF solution (Fig. 9) because of the formation

**Table 1**
Structure parameters of $PVEO_{17}$ cylindrical micelles formed in aqueous solutions obtained from the model fitting using Eq. (4).

| | $R_c$ (Å) | $N_r$ | $t_s$ (Å) | $L$ (Å) | $N_L$ | $\xi_d$ (Å) | $I_d(0)(cm^{-1})$ |
|---|---|---|---|---|---|---|---|
| 1 wt% | 5.38 ± 1.18 | 3.2 | 29.42 ± 2.02 | 348.94 ± 24.6 | 5.4 | 300.7 ± 11.1 | 13.14 ± 1.53 |
| 5 wt% | 7.5 ± 0.31 | 6.3 | 27.5 ± 0.09 | 360 ± 10.2 | 5.5 | 308 ± 7 | 28.36 ± 2.07 |
| 8 wt% | 8.37 ± 1.09 | 7.8 | 24.63 ± 0.58 | 380.08 ± 8.76 | 5.8 | 350.29 ± 10.2 | 49.17 ± 4.69 |

of cylindrical micelles. In this case, significant red-shift of the PL maximum is observed, implying that the DP-PPV aggregates in the micelles dominate the emission process. The peak located at 520 nm is attributed to the vibronic peak of the aggregate emission. The presence of this peak demonstrates that the chain packing or conformation is more ordered on forming the micelles in aqueous solution.

Fig. 10a shows the PL spectra of the aqueous solutions over a very broad concentration range. The PL maximum intensity remains virtually unaffected as the concentration is increased from $7.8 \times 10^{-4}$ to $1.5 \times 10^{-3}$ wt%, but the intensity increases progressively with increasing concentration above $1.5 \times 10^{-3}$ wt% (Fig. 10b). Moreover, the most intense peak is found to shift drastically to the lower energy (or longer wavelength) when the con-

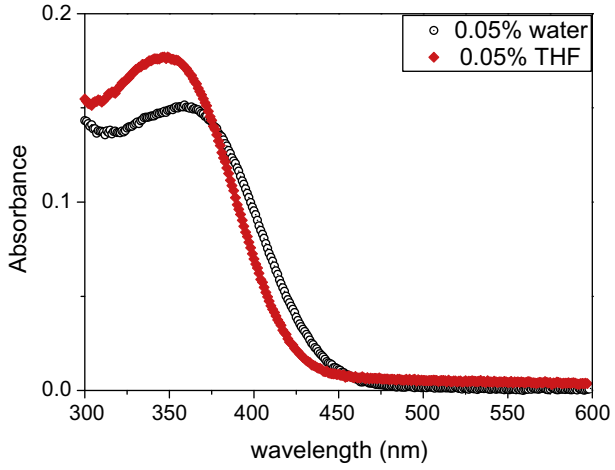


**Fig. 7.** UV–Vis spectra of $PVEO_{17}$ in the dilute solutions with THF and water (concentration = 0.05 wt%). The absorption peak is red shifted for the water solvent relative to that for the THF solvent.

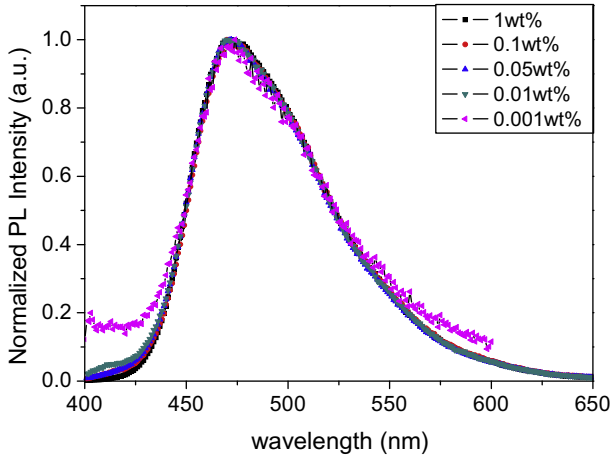


**Fig. 8.** PL spectra of $PVEO_{17}$ in THF solutions with various concentrations. The spectrum is virtually independent of concentration over the concentration range studied.

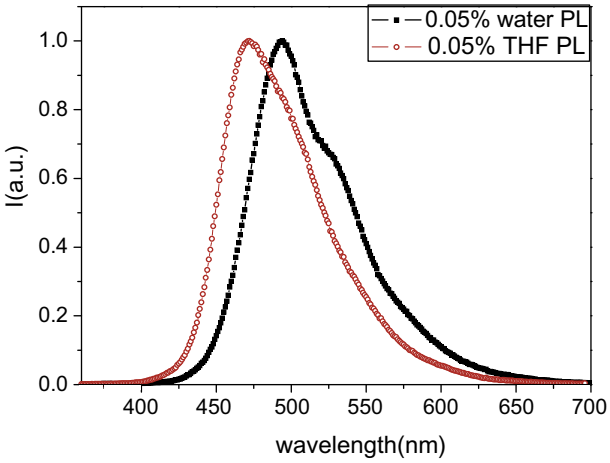


**Fig. 9.** PL spectra of $PVEO_{17}$ in dilute solutions with THF and water. The PL spectrum of aqueous solution changes obviously relative to that of the THF solution because of the formation of cylindrical micelles.

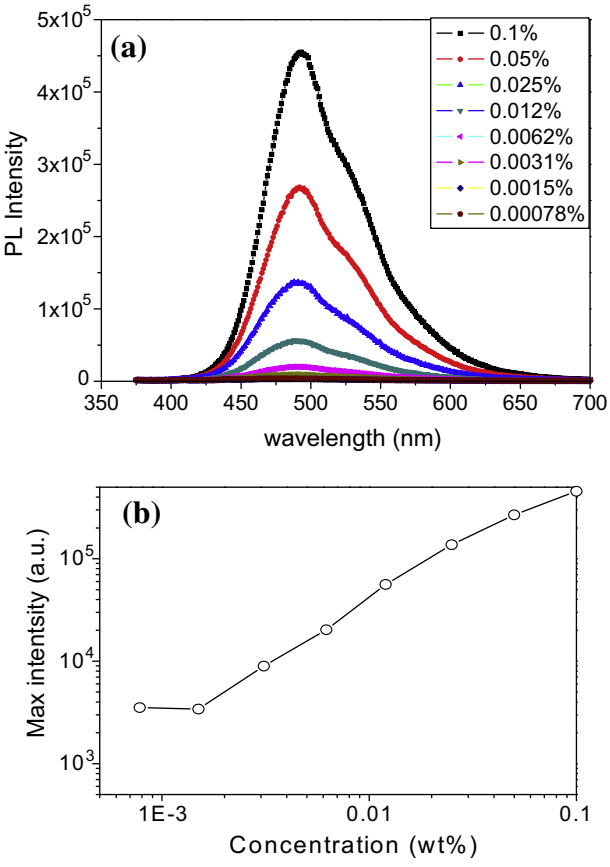


**Fig. 10.** (a) PL spectra of $PVEO_{17}$ in the aqueous solution with different concentrations. (b) PL maximum intensity as a function of concentration.

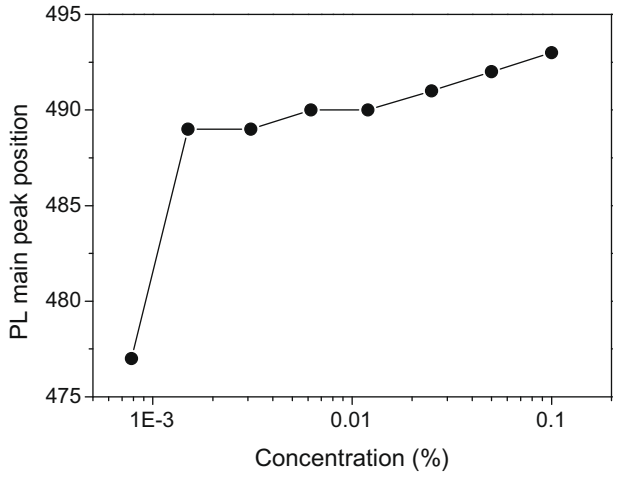


**Fig. 11.** PL main peak position as a function of concentration of $PVEO_{17}$ aqueous solution.

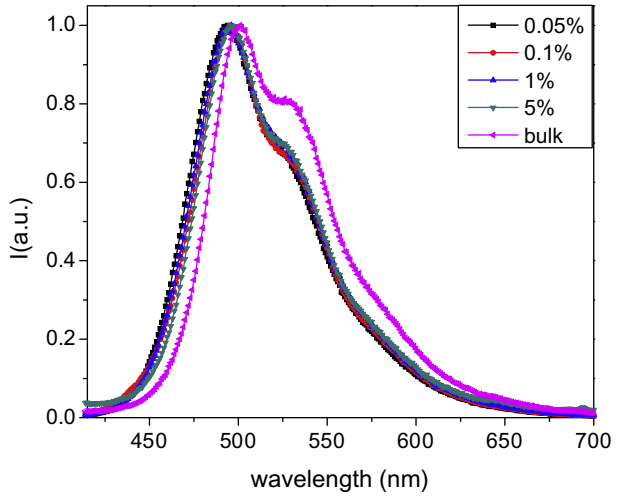


**Fig. 12.** Comparison of the PL spectra of the $PVEO_{17}$ aqueous solution with that of $PVEO_{17}$ in the bulk. The spectrum of the bulk sample is seen to display a strong red-shit (by 5 nm) relative to that of the solution samples.

centration is raised from $7.8 \times 10^{-4}$ to $1.5 \times 10^{-3}$ wt% (Fig. 11). As the concentration exceeds $1.5 \times 10^{-3}$ wt%, the red-shift becomes small. The results suggest that the micelles are probably not formed at the extremely low concentration of $7.8 \times 10^{-4}$ wt% and when the polymer concentration is raised to $1.5 \times 10^{-3}$ wt% the $PVEO_{17}$ chains aggregate to form cylindrical micelles, such that the aggregate emission becomes dominant in the PL spectra. Therefore, the critical micelle concentration should situate between $7.8 \times 10^{-4}$ and $1.5 \times 10^{-3}$ wt%.

Fig. 12 compares the PL spectra of the aqueous solution with that of $PVEO_{17}$ in the bulk. The spectrum of the bulk sample is seen to display a strong red-shit (by 5 nm) relative to that of the solution samples. The results suggest that the DP-PPV chains embedded within the core of the cylindrical micelles have a shorter conjugation length than those forming the disklike microdomains in the bulk state.

## 4. Conclusions

We have investigated the supramolecular structures of $PVEO_{17}$ in the bulk and solutions with THF and water. In the bulk state, the DP-PPV main chains packed to form disklike domains embedded in the matrix composing of the PEO side chains. The severe aggregation of DP-PPV backbone in the bulk state was manifested in the strong red-shift of the PL maximum relative to that of the polymer in the solution state. The PL spectra of the THF solution were essentially independent of concentration, signaling that single choromophore dominated the emission. However, SAXS revealed that the individual $PVEO_{17}$ chains dispersed in the THF solution displayed some degree of aggregation. Unlike the THF solution, $PVEO_{17}$ self-organized into cylindrical micelles in aqueous solution in the concentration range of 1–8 wt%. The aggregation number of the micelles increased with increasing concentration. The corresponding PL spectra showed a drastic red-shift when the concentration was raised from $7.8 \times 10^{-4}$ to $1.5 \times 10^{-3}$ wt%. As the concentration exceeded $1.5 \times 10^{-3}$ wt%, the red-shift became small, which suggested that the critical micelle concentration of $PVEO_{17}$ in water should situate between $7.8 \times 10^{-4}$ and $1.5 \times 10^{-3}$ wt%.

## Acknowledgement

This work was supported by the National Science Council (NSC) of Taiwan under the Grant No. NSC 97-2752-E-007-002-PAE and NSC 97-2221-E-007-034-MY3.

## References

[1] E.A. Minich, A.P. Nowak, T.J. Deming, D.J. Pochan, Polymer 45 (2004) 1951.
[2] B.D. Olsen, R.A. Segalman, Macromolecules 38 (2005) 10127.
[3] C. de Ruijter, W.F. Jager, L. Li, S.J. Picken, Macromolecules 39 (2006) 4411.
[4] J. Wu, E.M. Pearce, T.K. Kwei, A.A. Lefebvre, N.P. Balsara, Macromolecules 35 (2002) 1791.
[5] K. Loos, A. Boker, H. Zettl, M. Zhang, G. Krausch, A.H.E. Muller, Macromolecules 38 (2005) 873.
[6] M. Knaapila, B.P. Lyons, M. Torkkeli, A.P. Monkman, Adv. Funct. Mater. 16 (2006) 599.
[7] R. Stepanyan, A. Subbotin, M. Knaapila, O. Ikkala, G. ten Brinke, Macromolecules 36 (2003) 3758.
[8] R. Rulkens, G. Wegner, T. Thurn-Albrecht, Langmuir 15 (1999) 4002.
[9] A. Schmidt, K. Mathauer, G. Reiter, M.D. Foster, M. Stamm, G. Wegner, W. Knoll, Langmuir 10 (1994) 3820.
[10] F. Löscher, T. Ruckstuhl, T. Jaworek, G. Wegner, S. Seeger, Langmuir 14 (1998) 2786.
[11] S. Schwiegk, T. Vahlenkamp, Y. Xu, G. Wegner, Macromolecules 25 (1992) 2513.
[12] M. Bockstaller, W. Khler, G. Wegner, D. Vlassopoulos, G. Fytas, Macromolecules 33 (2000) 3951.
[13] A. Kroeger, V. Deimede, J. Belack, I. Lieberwirth, G. Fytas, G. Wegner, Macromolecules 40 (2007) 105.
[14] A. Kroeger, J. Belack, A. Larsen, G. Fytas, G. Wegner, Macromolecules 39 (2006) 7098.
[15] A. Gitsas, G. Floudas, G. Wegner, Phys. Rev. E 69 (2004) 041802.
[16] S.M. Fonseca, M.E. Eusébio, R. Castro, H.D. Burrows, M.J. Tapia, U. Olsson, J. Colloid Interf. Sci. 315 (2007) 805.
[17] M. Knaapila, L. Almasy, V.M. Garamus, C. Pearson, S. Pradhan, M.C. Petty, U. Scherf, H.D. Burrows, A.P. Monkman, J. Phys. Chem. B 110 (2006) 10248.
[18] D.D. Yeh, Master Thesis, National Chiao Tung University, Hsin-Chu, Taiwan, 2006.
[19] R.J. Roe, Methods of X-ray and Neutron Scattering in Polymer Science, Oxford University press, New York, 2000.
[20] O. Glatter, O. Kratky, Small Angle X-ray Scattering, Academic press, London, 1982.
[21] P. Debye, R. Anderson, H. Brumberger, J. Appl. Phys. 28 (1957) 679.
[22] P. Debye, A.M. Bueche, J. Appl. Phys. 20 (1949) 518.
[23] C.I. Huang, J.R. Chen, J. Polym. Sci. B 39 (2001) 270.
[24] Y.C. Li, K.B. Chen, H.L. Chen, Langmuir 22 (2006) 11009.
[25] I. Livsey, J. Chem. Soc., Faraday Trans. 2 83 (1987) 1445.
[26] P. Pang, P. Englezos, Polymer 204 (2002) 23.
[27] S. Verbrugghe, A. Laukkanen, V. Aseyev, H. Tenhu, F.M. Winnik, F.E. Du Prez, Polymer 44 (2003) 6807.
[28] S. Kinugasa, H. Nakahara, Macromolecules 27 (1994) 6889.
[29] A.M. Afifi-Effat, J.N. Hay, J. Polym. Sci., Polym. Lett. 9 (1971) 651.
[30] C. Lu, R. Pelton, Langmuir 20 (2004) 2962.
[31] B. Porsch, L.O. Sundelof, Macromolecules 28 (1995) 7165.
[32] D.A. Skoog, F.J. Holler, T.A. Nieman, Principles of Instrumental Analysis 5th, Thomson Learning, 1998.
[33] B.K. An, S.K. Kwon, S.Y. Park, Bull. Kor. Chem. Soc. 26 (2005) 1607.

[34] H. Becker, H. Spreitzer, K. Ibrom, W. Kreuder, Macromolecules 32 (1999) 4925.
[35] G. Padmanaban, S. Ramakrishnan, J. Am. Chem. Soc. 122 (2000) 2244.
[36] I.D.W. Samuel, B. Crystall, G. Rumbles, P.L. Burn, A.B. Holmes, R.H. Friend, Synth. Met. 54 (1993) 281.
[37] Z.Y. Hong, S. Lu, D.K. Wang, D.G. Ma, X.J. Zhao, L.X. Wang, N. Minami, N. Takada, Y. Ichino, K. Yase, X.B. Jing, F.S. Wang, Synth. Met. 102 (1999) 1134.
[38] Y.J. Miao, W.G. Herkstroeter, B.J. Sun, A.G. Wongfoy, G.C. Bazan, J. Am. Chem. Soc. 117 (1995) 11407.